



## Exploring the effect of longwave radiation exchange on the energy balance of building façades in subtropical regions

Cheng Zhao<sup>a</sup>, Lei Zhang<sup>a,\*</sup>, Yu Zhang<sup>b, \*\*</sup>

<sup>a</sup> State Key Laboratory of Subtropical Building Science, School of Architecture, South China University of Technology, 510640, Guangzhou, China

<sup>b</sup> Key Laboratory of Heat Transfer Enhancement and Energy Conservation of Education Ministry, School of Chemistry and Chemical Engineering, South China University of Technology, 510640, Guangzhou, China



### ARTICLE INFO

#### Keywords:

Longwave radiation  
Energy balance  
Radiation heat transfer  
Sensitivity analysis  
View factor

### ABSTRACT

The energy balance of the building façade affects the accuracy of building energy prediction. Although algorithms for energy balance have been applied in building energy simulation software, the longwave radiation exchange of building façades is often considered in a simple (implicit) way. This study proposes the concept of ambient equivalent temperature for quantifying the longwave radiation emitted by other buildings and trees in the surrounding environment. A more detailed radiation transfer model was developed to assess the energy balance of the longwave radiation of building façades. The input parameters of the model were simplified and the applicability of the model was improved by fitting the ambient equivalent temperature and meteorological parameters. Through quantitative and qualitative analysis, the effect of view factor parameters on the model output was assessed, and a universal value for the sky view factor (SVF) was determined to calculate the longwave radiation exchange of the building façade. The calculation accuracy of the longwave radiation was 71.4% higher in the simplified SVF model than in the original model. These findings provide a more accurate method for calculating the longwave radiation energy balance of building façades and have implications for building energy prediction and building energy efficiency design.

### 1. Introduction

Buildings account for approximately 40% of the world's total energy consumption, and reducing building energy consumption is one of the most crucial challenges of our time [1]. Accurate predictions of the energy consumption of buildings and evaluations of the energy-saving potential that can be achieved by building energy efficiency technologies are essential for reducing building energy consumption. Building energy simulation is a common method for assessing the energy of buildings based on dynamic heat balances [2]. Accurate prediction of building energy consumption can provide practitioners with guidelines that can help them make more informed decisions in the early design stages [3].

The thermotechnical parameters of the building envelope significantly affect the energy performance of buildings [4]. Detailed modeling of energy transfer allows for a better assessment of the thermal performance and energy loss of the building façade and enables more accurate predictions of the energy consumption of buildings [5].

According to building physics, the energy balance of the building façades is composed of three parts: conduction, natural convection, and thermal radiation [6]. The thermal radiation is further divided into two components: solar radiation and longwave radiation. In contrast to the properties of solar radiation, which can only be absorbed and reflected, the surface of a building wall absorbs, reflects, and emits longwave radiation. Therefore, calculations of longwave radiation exchange on the building façade are more complicated than calculations of solar radiation.

Although longwave radiation exchange is difficult to quantify in complex building environments, it has received extensive attention due to its important impacts in studies of urban heat islands [7], building energy simulation [8], and urban climate modelling [9]. In urban street canyons, radiation exchange between buildings is considered one of the main contributors to the urban heat island effect [10]. The reason for this is that in urban spaces with a high density of buildings, the mutual shading of buildings suppresses heat exchange between the building surfaces and the sky. Increases in the temperature of the building surfaces contribute to increases in the intensity of the urban heat island

\* Corresponding author.

\*\* Corresponding author.

E-mail addresses: [arzhang@scut.edu.cn](mailto:arzhang@scut.edu.cn) (L. Zhang), [arzy@scut.edu.cn](mailto:arzy@scut.edu.cn) (Y. Zhang).

Nomenclature	
Symbols	
SR	solar radiation [ $\text{W}/\text{m}^2$ ]
LR	longwave radiation [ $\text{W}/\text{m}^2$ ]
$LR_{\text{sky}}$	downward longwave radiation [ $\text{W}/\text{m}^2$ ]
SRC	standard regression coefficient [-]
TGP	treed gaussian process [-]
LHS	Latin hypercube sampling [-]
SSR	regression sum of squares [-]
SST	total sum of squares [-]
ARE	average relative error [-]
MBE	mean biased error [-]
RMSE	root mean square error [-]
MAPE	mean absolute percentage error [-]
var	variance [-]
E	expectation [-]
$R^2$	coefficient of determination [-]
SVF/ $F_{\text{sky}}$	sky view factor [-]
$F_g$	ground view factor [-]
$F_{\text{env}}$	view factor created by the obstruction [-]
$T_{\text{sky}}$	sky temperature [ $^\circ\text{C}$ ]
$T_f$	building façade temperature [ $^\circ\text{C}$ ]
$T_g$	ground temperature [ $^\circ\text{C}$ ]
$T_a$	air temperature [ $^\circ\text{C}$ ]
$T_{\text{env}}$	surface temperature of objects in the environment [ $^\circ\text{C}$ ]
$T_{\text{ae}}$	ambient equivalent temperature [ $^\circ\text{C}$ ]
$q_{\text{CD}}$	heat conduction [W]
$q_{\text{CV}}$	heat convection [W]
$q_{\text{SR}}$	solar radiation heat [ $\text{W}/\text{m}^2$ ]
$q_{\text{LR}}$	net longwave radiation heat [ $\text{W}/\text{m}^2$ ]
$R_n$	net longwave radiation of the building façade [ $\text{W}/\text{m}^2$ ]
$R_n'$	modified net longwave radiation of the building façade [ $\text{W}/\text{m}^2$ ]
$R_n''$	simplified net longwave radiation of the building façade [ $\text{W}/\text{m}^2$ ]
$R_s$	longwave radiation exchange of the building façade with the sky [ $\text{W}/\text{m}^2$ ]
$R_g$	longwave radiation exchange of the building façade with the ground [ $\text{W}/\text{m}^2$ ]
$R_{\text{in}}$	incident longwave radiation of the building façade [ $\text{W}/\text{m}^2$ ]
$LW_{p,i}$	predicted value of longwave radiation [ $\text{W}/\text{m}^2$ ]
$LW_{m,i}$	measured value of longwave radiation [ $\text{W}/\text{m}^2$ ]
$C$	cloud fraction [-]
$\bar{y}$	average value [-]
$y_i$	real value [-]
$f_i$	predicted value [-]
$S_i$	first-order sensitivity index [-]
$T_i$	total effect sensitivity index [-]
$X_i$	input parameter [-]
$X_{-i}$	other parameters [-]
$Y$	output value of the model [-]
$n$	the number of samples [-]
<i>Greek symbols</i>	
$\sigma$	Stefan–Boltzmann constant [-]
$\varepsilon_{\text{sky}}$	sky emissivity [-]
$\varepsilon_f$	emissivity of the ground [-]
$\varepsilon_g$	emissivity of the building façade [-]
$\varepsilon_{\text{env}}$	emissivity of objects in the environment [-]
$\theta$	angle between the wall and the ground [ $^\circ$ ]

effect.

In commonly used building energy simulation software (e.g., EnergyPlus), the longwave radiation balance of building façades is usually considered from the perspective of the individual building [11]. Although the thermal performance of the building façade has been assessed in detail through the development of numerical models, the effect of longwave radiation exchange between buildings on the energy balance of the building façade has not been considered [12]. In urban street canyons, the proximity of buildings to each other can generate complex thermal radiation fields, in which the building may become a heat source for adjacent buildings [13]. Longwave radiation is also captured by the building façade through multiple reflections between buildings, which significantly increases the total longwave radiation received by the building façade [14]. Ignoring this increase in longwave radiation can lead to errors in calculations of building energy consumption in urban spaces.

The original model built into EnergyPlus oversimplifies calculations of longwave radiation exchange of the building façade, as they only consider longwave radiation transfer to and from the sky and the ground [15]. This simplification is only suitable for open suburban areas and not applicable to densely built-up urban street canyons, where longwave radiation transfer from trees and other buildings in the surrounding environment requires consideration. Furthermore, the default setting generally assumes that the ground temperature and the surface temperature of surrounding buildings are equivalent to the air temperature from the meteorological data [16]. However, the air temperature has been shown to significantly differ from the building surface temperature, the ground temperature, and the canopy surface temperature in previous studies. Two regression models developed by Yadav et al. [17] for predicting outer wall temperatures revealed that building wall temperatures of different orientations and roof temperatures

significantly differed from air temperatures. Zhang et al. [18] measured the thermal performance of different types of green roofs in a subtropical monsoon climate and found that the temperature of green roofs was 7 °C higher than the air temperature in summer. Daily and monthly average ground temperatures measured at different depths by Tsilingiridis et al. [19] indicated that air temperatures were significantly lower than shallow ground surface temperatures. Miller et al. [20] measured the canopy temperature of trees at different heights in a tropical climate and found that the temperature at the uppermost part of the canopy was 5 °C higher than the air temperature. Cheung et al. [21] made remotely sensed measurements in Hong Kong of the tree canopy and below-canopy ground temperatures and found that both were lower than air temperatures. Therefore, this temperature simplification may lead to an underestimation or overestimation of the building façade temperature, which can affect calculations of longwave radiation energy balance and lead to errors in building energy prediction.

Another parameter that needs to be obtained when calculating the energy balance of a building façade is the view factor. The original model calculates the sky view factor (SVF) by dividing the sky dome into 144 points, which is a simpler and less accurate method [22]. Several improved methods have been subsequently proposed to improve accuracy. Jones et al. [23] proposed a digital graphic rendering method based on Monte Carlo simulations for calculating the view factor between two building surfaces. In the View3D tool, Luo et al. [24] developed a GPU-accelerated ray tracer and coupled it with EnergyPlus for calculating the view factor between high-density urban surfaces. Similarly, Xie et al. [25] used Monte Carlo ray-tracing methods to obtain the SVF and coupled it with EnergyPlus for predicting building energy performance and assessing the indoor thermal environment. Yang et al. [26] calculated the longwave radiation fluxes from the building façade and assessed the energy performance of the building by combining the

energy simulation software EnergyPlus and the microclimate simulation software ENVI-met. Miller et al. [27] coupled CitySim and EnergyPlus software and performed a co-simulation in which longwave radiation was calculated in CitySim and input into EnergyPlus to predict the building's heating and cooling loads. Although many scholars have calculated view factors in more detail using Monte Carlo ray-tracing methods or integrating the external calculation results from other software, obtaining view factors efficiently in complex scenes is still challenging due to limitations in computational resources. Furthermore, whether the accuracy of calculations of the longwave radiation on building façades can be improved by inputting accurate view factors remains unclear.

In this study, the ambient equivalent temperature was proposed to quantify the longwave radiation emitted from the surrounding environment, and a more detailed radiation transfer model was developed to simulate the longwave radiation exchange of the building façade. The emissivity and view factor parameters of the surrounding objects were simplified to improve the applicability of the longwave radiation model. Moreover, the effect of the view factor parameter on the longwave radiation transfer of the building façade was assessed through quantitative and qualitative analysis. Input values for the SVF were determined for rapid calculations of the longwave radiation exchange of the building façade, and the accuracy of the model was verified using various evaluation metrics.

## 2. Methodology

### 2.1. Longwave radiation exchange of building façades

It is generally agreed that the energy exchange of the external surface of a building wall is composed of four parts: conduction into the wall  $q_{CD}$ , convection with outdoor air  $q_{CV}$ , absorbed solar radiation  $q_{SR}$  and net longwave radiation  $q_{LR}$  [28]. When there is no change in the surface temperature of the building façade (i.e., no heat is stored/released), the energy balance of the building façade can be expressed as follows [29].

$$q_{CD} + q_{CV} + q_{SR} + q_{LR} = 0 \quad (1)$$

The calculation of net longwave radiation primarily takes into account the longwave radiation exchange of the building façade with the sky and the ground, as determined by Eq. (2) [30].

$$R_n = R_s + R_g \quad (2)$$

where  $R_n$  is the net longwave radiation on building façades ( $\text{W}\cdot\text{m}^{-2}$ ), and  $R_s$  and  $R_g$  are the longwave radiation exchange of the building façade with the sky and ground, respectively ( $\text{W}\cdot\text{m}^{-2}$ ).

According to the Stefan–Boltzmann law, which takes into account the view factor of the sky and ground and introduces the emissivity parameter of the building's external surface, Eq. (2) can be expressed in more detail as:

$$R_n = \sigma \epsilon_f \left( F_{sky} \left( T_{sky}^4 - T_f^4 \right) + F_g \epsilon_g \left( T_g^4 - T_f^4 \right) \right) \quad (3)$$

where  $\sigma$  is the Stefan–Boltzmann constant, the value of which is  $5.67 \times 10^{-8} \text{ W}\cdot\text{m}^{-2}\cdot\text{K}^{-4}$ ;  $\epsilon_f$  is the emissivity of the building façade;  $\epsilon_g$  is the emissivity of the ground;  $T_{sky}$ ,  $T_g$ , and  $T_f$  are the sky temperature, ground temperature, and building façade temperature, respectively ( $^\circ\text{C}$ ).  $F_{sky}$  and  $F_g$  are the sky view factor and ground view factor, respectively, which are calculated as follows [31]:

$$F_{sky} = 0.5(1 + \cos \theta) \quad (4)$$

$$F_g = 0.5(1 - \cos \theta) \quad (5)$$

where  $\theta$  is the angle between the wall and the ground ( $^\circ$ ). For building façades, both  $F_{sky}$  and  $F_g$  take the value of 0.5.

The sky temperature, sometimes referred to as the sky effective temperature [32], is calculated by Eq. (6) and Eq. (7).

$$T_{sky} = \left( \frac{LR_{sky}}{\sigma} \right)^{0.25} \quad (6)$$

$$LR_{sky} = \epsilon_{sky} \sigma T_a^4 \quad (7)$$

where  $LR_{sky}$  is the downward longwave radiation ( $\text{W}\cdot\text{m}^{-2}$ );  $T_a$  is the air temperature ( $^\circ\text{C}$ ); and  $\epsilon_{sky}$  is the sky emissivity, which is an important parameter for assessing the ability of the sky to emit longwave radiation.

In EnergyPlus software,  $\epsilon_{sky}$  for sunny days is calculated using the Walton model [33]; calculations of  $\epsilon_{sky}$  on cloudy days require the introduction of the cloud fraction  $C$ , which is calculated using the Clark and Allen model [34]. The exact formula can be found in the EnergyPlus help file. Similarly, the sky temperature is calculated using the above parameters in TRNSYS software with the formula in Eq. (8) [35].

$$T_{sky} = T_a (\epsilon_{sky} + 0.8C(1 - \epsilon_{sky}))^{0.25} \quad (8)$$

The cloud fraction is a parameter used to quantify the degree of cloudiness and is typically given a value between 0 and 1. As the rooftop weather station is not equipped for cloud observation, the  $LR_{sky}$  is obtained directly from the Pyrgeometer instead of being calculated by Eq. (7) and Eq. (8).

Eq. (3) to Eq. (5) are only applicable to a simple environment where there are no trees or other buildings. When calculating the energy balance of a building façade in a complex environment, it is necessary to consider the longwave radiation exchange from the surfaces of objects (e.g., other building surfaces) in the surrounding environment.

As a result, the net longwave radiation from the building façade can be modified to Eq. (9), where the relationship between view factors can be expressed by Eq. (10).

$$R_n' = \sigma \epsilon_f \left( F_{sky} \left( T_{sky}^4 - T_f^4 \right) + F_g \epsilon_g \left( T_g^4 - T_f^4 \right) + F_{env} \epsilon_{env} \left( T_{env}^4 - T_f^4 \right) \right) \quad (9)$$

$$F_{sky} + F_g + F_{env} = 1 \quad (10)$$

Where  $T_{env}$  is the surface temperature of objects in the environment ( $^\circ\text{C}$ );  $\epsilon_{env}$  is the emissivity of objects in the environment; and  $F_{env}$  is the view factor created by the obstruction.

In previous research, the ground temperature and the surface temperature of other buildings are approximated using the air temperature [22]. However, in actual environments, the ground temperature and the surface temperature of other buildings are not equal to the air temperature due to solar radiation and other factors [36]. Therefore, the parameter of ambient equivalent temperature  $T_{ae}$  is introduced in this study to determine the longwave radiation exchange between the building façade and the ground and between the surface of other objects in the surrounding environment. The new concept of ambient equivalent temperature is derived from the concept of equivalent temperature, which is used to calculate the radiation of celestial bodies. This concept assumes that all objects in the surrounding environment are a blackbody with an emissivity of 1. The ability of other objects in a complex environment to emit longwave radiation is assessed using this simplified parameter.

$$R_n'' = \sigma \epsilon_f \left( F_{sky} \left( T_{sky}^4 - T_f^4 \right) + (1 - F_{sky}) \left( T_{ae}^4 - T_f^4 \right) \right) \quad (11)$$

Eq. (11) combines the temperature parameters  $T_g$  and  $T_{env}$  and introduces the concept of equivalent black bodies to remove the emissivity parameters for different surfaces. The input parameters for the view factor are simplified by combining the view factors of the ground and the environment. The simplified SVF is a parameter that ranges from 0 to 0.5, and the incident longwave radiation of the building façade is shown in Eq. (12).

$$R_{in} = \sigma \left( F_{sky} T_{sky}^4 + (1 - F_{sky}) T_{ae}^4 \right) \quad (12)$$

The model was tested in subsequent studies, and the relationships between ambient equivalent temperature and meteorological parameters were established.

## 2.2. Field measurements

### 2.2.1. Experimental setting

The experimental site comprised the outdoor environment near the Building Energy and Environment Laboratory of the South China University of Technology in Guangzhou, China. Guangzhou ( $23^{\circ}1'N$ ,  $113^{\circ}3'E$ ) has a subtropical monsoon climate characterized by warm and rainy weather, abundant light and heat, long summers, and short frost periods.

Given the difficulty of finding an environment varying in the SVF at a fixed location on the building façade, a special method was used to measure incident longwave radiation on building façades. The specific method involved first finding different SVF scenes in the outdoor environment (detailed calculations of SVF are provided in section 2.2.2); the Pyrgeometer was then mounted vertically on a tripod and placed in a scene where the specific value of SVF is known. In this case, the longwave radiation measured by the probe is the incident longwave radiation of the hypothetical building façade. The Pyrgeometer was mounted at a height of 1.5 m above ground level to simulate the first-floor façade of a building; an image of the apparatus used to take measurements and the installation of the instruments are shown in Fig. 1 (a) and (b), respectively.

To investigate the effect of the SVF parameter on the longwave energy balance of building façades, five sites with SVFs ranging from 0.1 to 0.5 were selected for field measurements. The different SVF measurement scenes are shown in Fig. 1(c). Unfortunately, some of the experimental data for location E were lost due to Typhoon Chaba during the field measurements. Therefore, to obtain data equivalent to the amount that was lost, an additional location F with the same SVF was subsequently added, and measurements were taken at this location.

To avoid the adverse effects of a single experimental environment on longwave radiation measurements, the test scenes included four components: sky, ground, building surfaces, and trees. In addition, the effect of building height was also considered during the selection of

measurement locations. Therefore, the incident longwave radiation from the building façade was measured on the second floor and the roof of the building.

Six experiments were conducted in 2022 from 9 June to 30 September. Measurements in each experiment were conducted continuously for seven days, and time-by-minute data on incident longwave radiation were obtained for a total of six different scenes. The longwave radiation was measured using a Pyrgeometer (CGR3, Kipp & Zonen, Netherlands), and the data were recorded in a data logger (CR1000, Campbell Scientific Inc., UT, USA).

In addition, a weather station was installed on the roof of the Building Energy and Environment Laboratory to obtain meteorological data during field measurements. This weather station allows the acquisition of 10 common meteorological parameters: air temperature, relative humidity, wind speed, wind direction, pressure, precipitation, direct solar radiation, total solar radiation, scatter solar radiation, and downward longwave radiation. Table 1 shows the details of the equipment used to obtain meteorological parameters; the current status of the weather station is shown in Fig. 2.

### 2.2.2. SVF of building façades

For an urban street canyon, the SVF is the ratio of the visible sky area to the total sky area at a location [37]. In open areas, the value is close to 1; in built-up urban areas, it is below 1. This parameter is important for calculating the solar radiation and longwave radiation balance [38]. Five main methods have been used to calculate and evaluate the SVF [39]: geometric methods, fish-eye photography methods, GPS methods,

**Table 1**  
Summary of weather station equipment.

Parameters	Manufacturer and model	Accuracy
Air temperature	Campbell CS215	$\pm 0.4^{\circ}\text{C}$
Relative humidity		$\pm 2\%$
Wind speed	R.M. Young 81000	$\pm 1\%$
Wind direction		$\pm 2^{\circ}$
Precipitation	Campbell TE525MM	$\pm 1\%$
Direct solar radiation	K&Z SOLYS2	$\pm 0.5\%$
Total solar radiation	K&Z CMP3	$\pm 5.0\%$
Scatter solar radiation	K&Z CMP3	$\pm 5.0\%$
Longwave radiation	K&Z CGR4	$\pm 5.0\%$

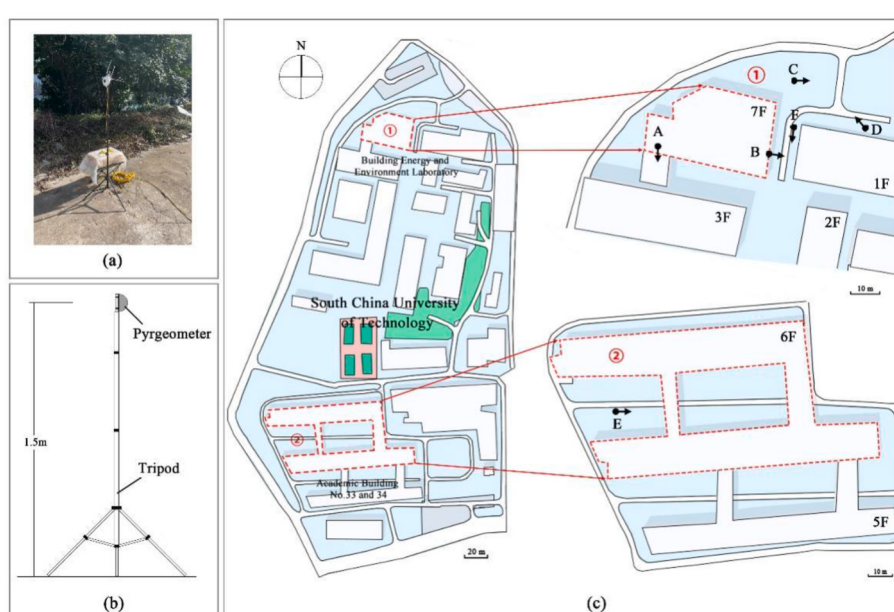


**Fig. 1.** Field measurements: (a) image of the apparatus used to take measurements; (b) installation of the instruments; (c) experimental sites (A–F).



**Fig. 2.** Weather station.

simulation methods based on digital surface models and 3D city models, and big data approaches from street view images.

The geometric method is a more accurate theoretical calculation method, but it can only be applied to simple and regular scenes [40]. Although the SVF can be batch-calculated using GPS methods, simulation methods, and big data approaches, the computational accuracy of these methods is lower than that of the fish-eye photography method [41]. The fish-eye photography method was thus used for SVF calculations. One of the major advantages of this method is that it accounts for the effects of trees.

In our study, a digital camera (EOS60D, Canon, Japan) with a CMOS sensor ( $22.3 \times 14.9$  mm) and an effective pixel count of approximately 17.9 million was used. It was equipped with a fisheye lens with a focal length of 4.5 mm to obtain images of the experimental site. Images were typically taken in the street canyon with the camera lens positioned horizontally upwards, and then the SVF was calculated through image processing to quantify the shading by buildings and trees in the

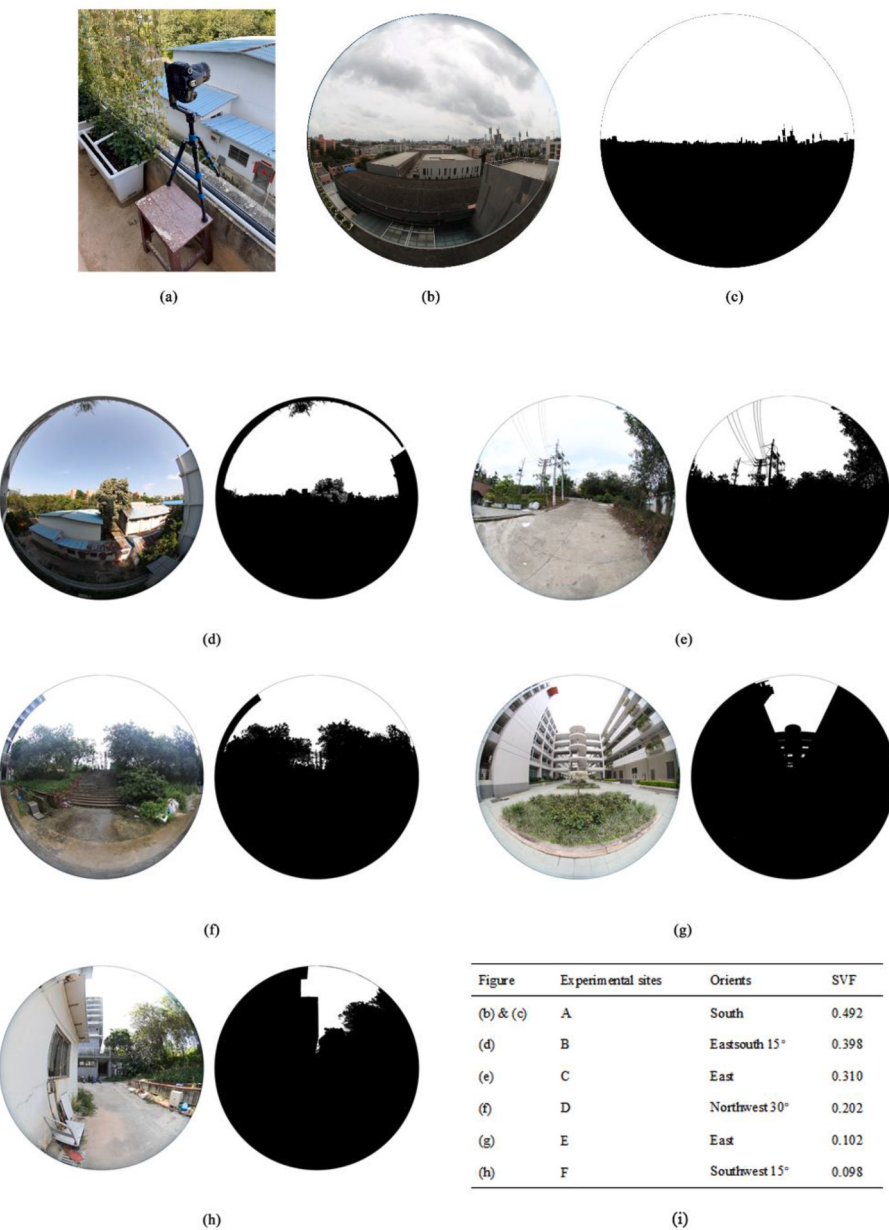


**Fig. 3.** SVF measurement methods and calculations for different experimental sites: (a) position of the camera; (b) original image of site A; (c) binarized processed image of site A; (d) images of site B; (e) images of site C; (f) images of site D; (g) images of site E; (h) images of site F; (i) summary of the orientation and results.

surrounding environment. This process accounts for the entire hemispheric sky and does not take into account the ground view factor. However, when measuring the view factor of a building façade, both the quarter sphere sky as well as the ground percentage require consideration. For this reason, the camera was placed vertically, ensuring that the direction of the lens normal was parallel to the horizontal during measurements. To ensure the stability of the shots, the camera was mounted on a manually controlled swivel tripod, as shown in Fig. 3 (a).

The images were captured in different scenes and then binarized using ImageJ software [42], and the sky and other objects were labelled using white pixels and black pixels, respectively. Fig. 3(b) and (c) show the results before and after image processing, respectively, and the SVF images for the other scenes are shown in Fig. 3(d)–(h). The specific SVF values are calculated by measuring the ratio of white pixels to black pixels, and the results are summarized in Fig. 3(i).

### 2.3. Evaluation

#### 2.3.1. Sensitivity analysis

Sensitivity analysis is required to explore the effect of each input parameter in the model on the calculations of incident longwave radiation from building façades. Sensitivity analysis is a method for investigating how uncertainty in the model input parameters affects the model output; sensitivity analyses can be divided into two categories: global sensitivity analysis and local sensitivity analysis [43]. The former evaluates all input parameters simultaneously and analyses the extent to which each variable contributes to the final calculated result, while the latter analyses the magnitude of the influence of each input variable on the output result on a case-by-case basis while holding the other input variables constant [44].

Compared with local sensitivity analysis, global sensitivity analysis has significant advantages in that it can determine the effect of each parameter and the interactions between parameters on the model output results when multiple parameters are varied together. The main methods of global sensitivity analysis include regression analysis, screening-based methods, variance-based methods, and meta-model-based methods [45].

Regression analysis has the advantage of being computationally fast and easy to understand, and it is widely used in building thermal performance assessments, especially the standard regression coefficient (SRC) method [46,47]. However, a prerequisite for the use of this method is a linear relationship between the individual input parameters and the results of the model calculation. Therefore, the coefficient of determination ( $R^2$ ) needs to be calculated to determine the linearity of the model as follows.

$$R^2 = \frac{SSR}{SST} = 1 - \frac{\sum_{i=1}^n (y_i - \bar{y})^2}{\sum_{i=1}^n (f_i - \bar{y})^2} \quad (13)$$

where SSR is the regression sum of squares; SST is the total sum of squares;  $\bar{y}$  is the average value;  $y_i$  is the real value; and  $f_i$  is the predicted value. This sensitivity method can be used when  $R^2 \geq 0.7$  [43], and the details of the linearity assessment are given in Section 3.3.

Meta-model-based sensitivity analysis methods can be used when exploring non-linear sensitivity relationships [48]. In this paper, the treed gaussian process (TGP), which is a machine learning method that combines a Gaussian process and a decision tree, was used to analyse the longwave radiation model. TGP can better handle non-linear dynamic models compared with other methods.

The TGP sensitivity analysis method permits the first-order and total effects to be determined, with larger values of these two indices indicating a greater influence of the parameter on the model output. The first-order sensitivity index  $S_i$  refers to the ratio of variance resulting from each parameter acting alone to the total variance, while the total effect sensitivity index  $T_i$  refers to the ratio of variance resulting from multi-parameter interactions to the total variance; both indices have

values between 0 and 1. The specific formulas are as follows [49].

$$S_i = \frac{\text{var}(E(Y|X_i))}{\text{var}(Y)} \quad (14)$$

$$T_i = 1 - \frac{\text{var}(E(Y|X_{-i}))}{\text{var}(Y)} \quad (15)$$

where  $X_i$  is the input parameter;  $X_{-i}$  represents the other parameters;  $Y$  is the output value of the model; var is the variance; and E is the expectation.

To better verify the sensitivity of each parameter, the Latin hypercube sampling (LHS) method was used to generate the parameters and combine them with the output of the model into sampling units. The LHS is a popular method for achieving a uniform distribution of the sampling results over space that can avoid duplicate sampling [50]. The sensitivity analysis, LHS, and data processing described above were implemented in RStudio software.

#### 2.3.2. Model validation

Aside from the sensitivity analysis, which is a qualitative method for evaluating the relationship between the effects of model inputs and outputs, the accuracy of the model needs to be verified using quantitative indicators [51]. Therefore, three indicators, mean biased error (MBE), root mean square error (RMSE), and mean absolute percentage error (MAPE), were used to evaluate the accuracy of the model. The MAPE parameter allows for a more objective quantification of error and provides an intuitive interpretation of the model.

$$\text{MBE} = \frac{\sum_{i=1}^n (LW_{m,i} - LW_{p,i})}{n} \quad (16)$$

$$\text{RMSE} = \left( \frac{\sum_{i=1}^n (LW_{m,i} - LW_{p,i})^2}{n} \right)^{0.5} \quad (17)$$

$$\text{MAPE} = \frac{\sum_{i=1}^n \left| \frac{LW_{m,i} - LW_{p,i}}{LW_{m,i}} \right|}{n} \quad (18)$$

where  $LW_{p,i}$  is the predicted value of longwave radiation ( $\text{W}\cdot\text{m}^{-2}$ );  $LW_{m,i}$  is the measured value of longwave radiation ( $\text{W}\cdot\text{m}^{-2}$ ); and  $n$  is the number of samples.

The longwave radiation data collected from the field measurements for model fitting were mainly concentrated in the summer months when temperatures are high. Therefore, the validation data were obtained from previous field measurements in the autumn and spring. The field measurements were carried out in November 2021 and March 2022, and a more detailed description of the field measurements is provided in Ref. [52].

## 3. Results and analysis

### 3.1. Selection of meteorological parameters and correlation tests

Meteorological data throughout the experiment were obtained through a weather station on the roof of the State Key Experimental Building for Subtropical Building Science, and the data are shown in Table 2. All six measurement points are no more than 300 m from the weather station; thus, data from this weather station provide a good representation of the weather conditions of all the experimental sites.

The data in the table show that the average values of the air temperature and relative humidity were  $29.51^\circ\text{C}$  and 80.87%, respectively. This indicates that the air temperature and relative humidity during the experimental period were high, which reflects the hot and humid conditions of a typical summer in a subtropical region. Furthermore, the other parameters essentially span the range of meteorological parameters that Guangzhou typically experiences throughout the year.

**Table 2**  
Summary of meteorological parameters during field measurements.

Parameters	Range	Average
Air temperature (°C)	24.11–35.93	29.51
Relative humidity (%)	45.82–100	80.87
Wind speed (m·s <sup>-1</sup> )	0.76–4.99	2.42
Wind direction (°)	2.46–359.30	140.86
Pressure (hPa)	965–977	969
Precipitation (mm·h <sup>-1</sup> )	0–23.6	0.31
Direct solar radiation (W·m <sup>-2</sup> )	0–751.1	179.28
Total solar radiation (W·m <sup>-2</sup> )	0–999	263.31
Scatter solar radiation (W·m <sup>-2</sup> )	0–588.1	156.55
Longwave radiation (W·m <sup>-2</sup> )	409–478.9	442.53

Using the incident longwave radiation data obtained from field measurements, the longwave radiation emitted by the environment was inverted by substituting the SVF parameters at different locations into Eq. (12). In this case, the sky longwave radiation was obtained using a rooftop weather station. The ambient equivalent temperature was calculated according to Stephen Boltzmann's law and Planck's law of blackbody radiation.

The ambient equivalent temperature is a newly proposed and important parameter for assessing the longwave radiation emitted by the environment. According to the results of previous and current data, the ambient equivalent temperature is always higher than the air temperature, especially during the daytime [52]. Therefore, this simplified method needs to be optimized to minimize errors during radiation calculations.

Meteorological parameters are important input parameters for assessing building energy consumption. Therefore, linear regressions of the six conventional meteorological parameters air temperature, relative humidity, direct solar radiation, total solar radiation, wind speed, and longwave radiation against the ambient equivalent temperature were conducted. The fitting results are shown in Fig. 4.

The highest linear correlation was observed between air temperature and the ambient equivalent temperature ( $R^2 = 0.81$ ). This indicates that the use of air temperature to replace the ambient equivalent temperature is justified to some extent, but this requires correction by adding coefficients and other parameters. For example, Ge et al. [53] calculate the ground temperature based on heat transfer by adding other parameters to the air temperature.

Furthermore, the results show that linear correlations of relative humidity, direct solar radiation, and total solar radiation with the ambient equivalent temperature were strong. Thus, accurate assessment of longwave radiation emitted by the environment requires consideration of the effects of multiple meteorological parameters. Equations for calculating the ambient equivalent temperature were developed using multiple linear regression per Ouzzane et al. [54]. Due to the weak linear relationship of wind speed and longwave radiation with ambient equivalent temperature ( $R^2$  of 0.24 and 0.18, respectively), these two parameters were not considered in the multiple linear fit.

Theoretical analysis revealed an intrinsic relationship between direct solar radiation and total solar radiation; therefore, only the total solar radiation, which had the higher  $R^2$  value, was used in the multiple linear fit. In subsequent models, relative humidity was eliminated to reduce model complexity because although its  $R^2$  value was high, its effect on the equivalent ambient temperature did not exceed 0.1 °C. Therefore, only air temperature and total solar radiation were used in the multiple linear regression.

### 3.2. Multiple regression of ambient equivalent temperature

In building energy simulation software (e.g., EnergyPlus), the ambient equivalent temperature is not a parameter that can be input directly. For energy balance calculations of building façades, only parameters from weather files are typically used as input parameters for

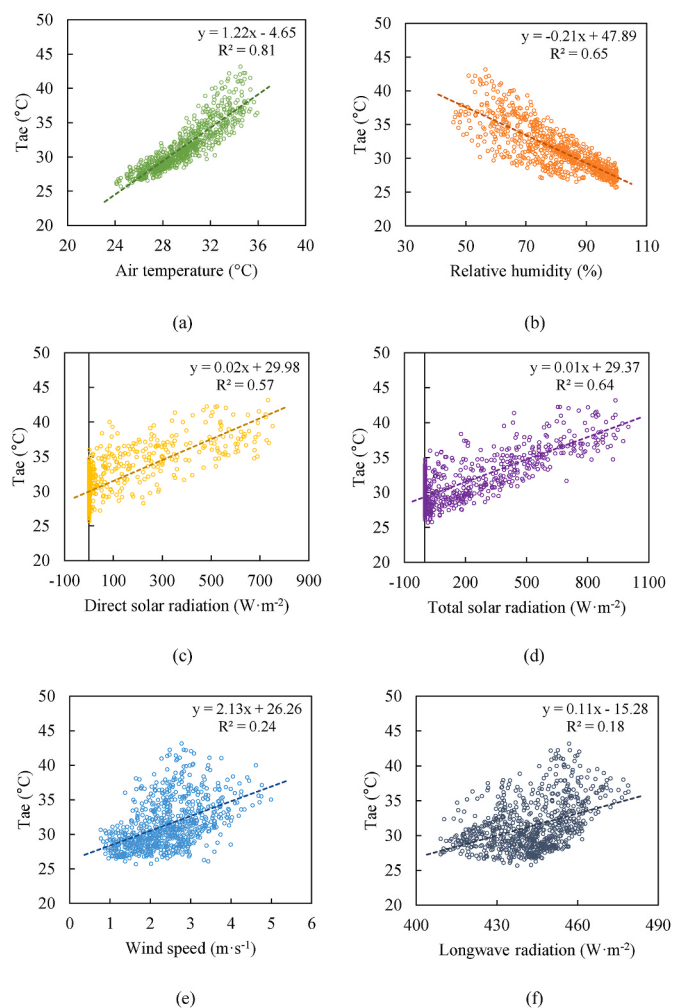


**Fig. 4.** Linear correlations between ambient equivalent temperature and different meteorological parameters: (a) air temperature; (b) relative humidity; (c) direct solar radiation; (d) total solar radiation; (e) wind speed; (f) longwave radiation.

energy evaluation [55]. Therefore, when calculating the incident longwave radiation on the building façade, the parameter of ambient equivalent temperature needs to be input through conversion of normal meteorological parameters.

The ambient equivalent temperature was calculated for six scenes with different SVFs, and multiple linear regression was performed using air temperature and solar radiation data collected from weather stations. The results of the three-dimensional fits are shown in Fig. 5.

As can be seen from the figure, the best fit was achieved for the data with an SVF of 0.202 ( $R^2 = 0.963$ ), followed by an SVF of 0.398 ( $R^2 = 0.953$ ). Compared with the results of the linear regression method in the previous section, in which the air temperature parameter was used, the inclusion of the solar radiation parameter greatly increased the  $R^2$  value of the fitted results. The reason is that the surface temperature of the ground and other building surfaces is significantly increased during the daytime by exposure to sunlight. Therefore, the effect of solar radiation needs to be considered when fitting the ambient equivalent temperature. Using both parameters, air temperature and solar radiation, to calculate the equivalent ambient temperature enhances accuracy.

In addition, the lowest  $R^2$  values were observed when the SVF was equal to 0.102, which was due to the effects of Typhoon Chaba during the field measurements. As a result, the measured incident longwave radiation values are small, and this leads to an underestimation of the ambient equivalent temperature in the subsequent calculations and an

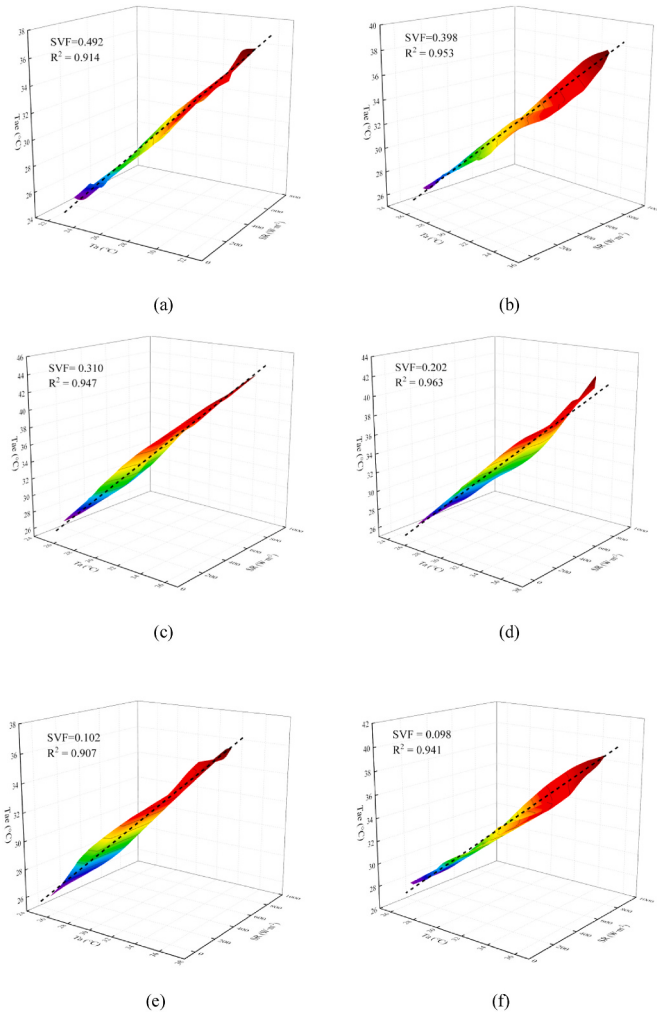


**Fig. 5.** Results of the multiple linear regression for different SVF scenes: (a) site A with SVF = 0.492; (b) site B with SVF = 0.398; (c) site C with SVF = 0.310; (d) site D with SVF = 0.202; (e) site E with SVF = 0.102; (f) site F with SVF = 0.098.

inferior fit compared with other SVF scenes.

Consequently, measurements were taken from an additional site with a similar SVF, and the fitted formulas for all the SVF scenes are summarized in Table 3.

Accurate SVFs are difficult to obtain in different scenes, and SVFs in the actual environment might not exactly match those in Table 3. Therefore, all data collected during experiments were fitted to determine a universal formula. To remove the effect of extreme weather on the data, data from location F with the same SVF were used rather than

**Table 3**  
Summary of the fitting results for the different locations.

Locations	SVF	Formulas	R <sup>2</sup>
A	0.492	Tae = 1.066 Ta + 0.007 SR	0.914
B	0.398	Tae = 1.004 Ta + 0.009 SR	0.953
C	0.310	Tae = 1.055 Ta + 0.010 SR	0.947
D	0.202	Tae = 1.016 Ta + 0.008 SR	0.963
E	0.102	Tae = 1.009 Ta + 0.005 SR	0.907
F	0.098	Tae = 1.025 Ta + 0.007 SR	0.941

The coefficient values for air temperature varied considerably among formulas, which indicates that air temperature has an important influence on calculations of longwave radiation emitted by the environment. However, a theoretical basis supporting this conjecture is lacking; a sensitivity analysis was thus carried out in Section 3.3 to evaluate the effect of air temperature.

data from location E. The universal formula for calculating the ambient equivalent temperature is as follows.

$$\text{Tae} = 1.031 \text{ Ta} + 0.008 \text{ SR} \quad (20)$$

The  $R^2$  value of the fitted formula is 0.893, which is lower compared with the formula for different SVF scenes, but it is still within a reasonable range. The formula was obtained by fitting the data collected under different SVF scenes, and field measurements were conducted in the hot summer season. Therefore, this formula is well applicable to subtropical regions.

### 3.3. Impact analysis of input parameters on model performance

Three meteorological parameters and the SVF were used to assess the exchange of longwave radiation from the building façade, but the effect of each parameter on the energy balance of the building façade remains unclear. Consequently, the contribution of the model's input parameters to the uncertainty in the longwave radiation calculations of the building façade needs to be determined.

The SVF parameter calculated in this paper was obtained by taking pictures of a specific scene, but it cannot be directly obtained from existing models from building simulation software [25]. To enhance the usefulness and generalizability of the model, the SVF parameter should be entered as a deterministic parameter. Therefore, a sensitivity analysis needs to be conducted to determine the effect of the SVF parameter on the longwave radiation model and to determine the best input value for the SVF.

The longwave radiation model used for sensitivity analysis has a total of four input parameters: air temperature, total solar radiation, downward longwave radiation, and the SVF. First, LHS was conducted. The range of values for all parameters was set according to the meteorological data from the weather station for the entire year of 2021 (Table 4).

The sampling range of all parameters is based on the following principle: the value range of meteorological parameters is a subset of the sampling value range. The sample size of the LHS is generally set according to the principle of at least 10 variations of a parameter [56], but to make the results of the sensitivity analysis more accurate, sampling was carried out 500 times in this study.

In addition, the accuracy of the sensitivity analysis results can only be ensured if all variables are independent [49]. Therefore, correlations between the input variables need to be verified before conducting a sensitivity analysis. In this paper, Pearson correlation tests were conducted, and the results are shown in Table 5.

The p-values between all the input parameters are much greater than 0.05, and the Pearson correlations between all the parameters are small, with an absolute value of no more than 0.1. This indicates that there is no correlation between all the input parameters and thus that the requirements of the input parameters for the sensitivity analysis are met.

In addition, the  $R^2$  between the output of the longwave radiation model and each input parameter was calculated (Table 5). Only the  $R^2$  between the air temperature and the model output was greater than or equal to 0.7, and the  $R^2$  of the remaining three parameters was less than 0.7. This indicates that the longwave radiation model in this paper is not suitable for the SRC sensitivity analysis method [57]; thus, the TGP

**Table 4**  
Range of meteorological parameters for 2021 and the sampling ranges.

Parameter	Range of meteorological data	Range of values for samples
Air temperature (°C)	5.06–38.84	5–40
Total solar radiation (W·m <sup>-2</sup> )	0–1020	0–1020
Longwave radiation (W·m <sup>-2</sup> )	242.8–484.7	240–485
SVF		0–0.5

**Table 5**

Results of Pearson correlations between input parameters and  $R^2$  for the model output.

Parameters		Ta	SR	LR	SVF
Ta	Pearson correlation	1	0.032	-0.057	-0.038
	P-value	-	0.479	0.206	0.386
SR	Pearson correlation		1	0.068	0.074
	P-value		-	0.131	0.100
LR	Pearson correlation			1	0.001
	P-value			-	0.981
SVF	Pearson correlation				1
	P-value				-
Model output	$R^2$	0.749	0.024	0.084	0.071

method was used to determine the sensitivity of each input parameter.

To facilitate comparison of the sensitivities of the different parameters, the output of the model was standardized. The range of responses was between -0.5 and 0.5, and the results of the sensitivity analysis are shown in Fig. 6.

The slope of the air temperature curve remained essentially constant, indicating that there was a linear relationship between air temperature and the model output. Although the slopes of the other three parameters fluctuate slightly with the input parameters, the overall relationship between these three parameters and the model output is also approximately linear. In addition, the positive and negative values of the slope revealed positive correlations among all three parameters, except for the SVF, which was negatively correlated with the model output.

Furthermore, the specific values in the main effects plot revealed that the parameter with the greatest influence on the model calculations was air temperature, followed by downward longwave radiation and the SVF; the least influential factor was total solar radiation. The results of the first-order and total effect indices also show that air temperature was the dominant parameter affecting the model output, which accounts for

approximately 80% of the output variance. This result confirms the conjecture in section 3.2.

Although the results show that solar radiation was the least influential factor, the fitted Eq. (20) shows that a  $100 \text{ W m}^{-2}$  change in solar radiation will cause a  $0.8^\circ\text{C}$  change in the equivalent ambient temperature. Ignoring solar radiation would thus result in a significant underestimation of the daytime equivalent ambient temperature. Downward longwave radiation is a direct parameter used to calculate the energy balance of the building façade that also requires consideration.

Therefore, the model can only be simplified in terms of the SVF to enhance its applicability. However, a qualitative analysis of sensitivity alone is not sufficient for clarifying the impact of the SVF; thus, the specific impact of this parameter needs to be quantified through experimental data. To this end, the average relative error between the simulated and measured values was calculated using longwave radiation data measured in six different SVF scenes and by varying the input values of the SVF of the model. The results are shown in Fig. 7.

The figure shows that all the average relative errors were less than 5.00%, regardless of the variation in input SVF values. This indicates that SVF has a small effect on calculations of longwave radiation from the building façade. Therefore, to simplify this longwave radiation model, an input SVF value that can be used in all scenes was finally determined based on the analysis shown in Fig. 7. When the SVF is equal to 0.236, an average relative error of less than 1.90% can be achieved for all cases.

This result provides an effective solution for addressing the errors caused by SVF approximations in previous studies [16]. A universal value is provided to reasonably simplify calculations of longwave radiation on building façades while maintaining calculation accuracy.

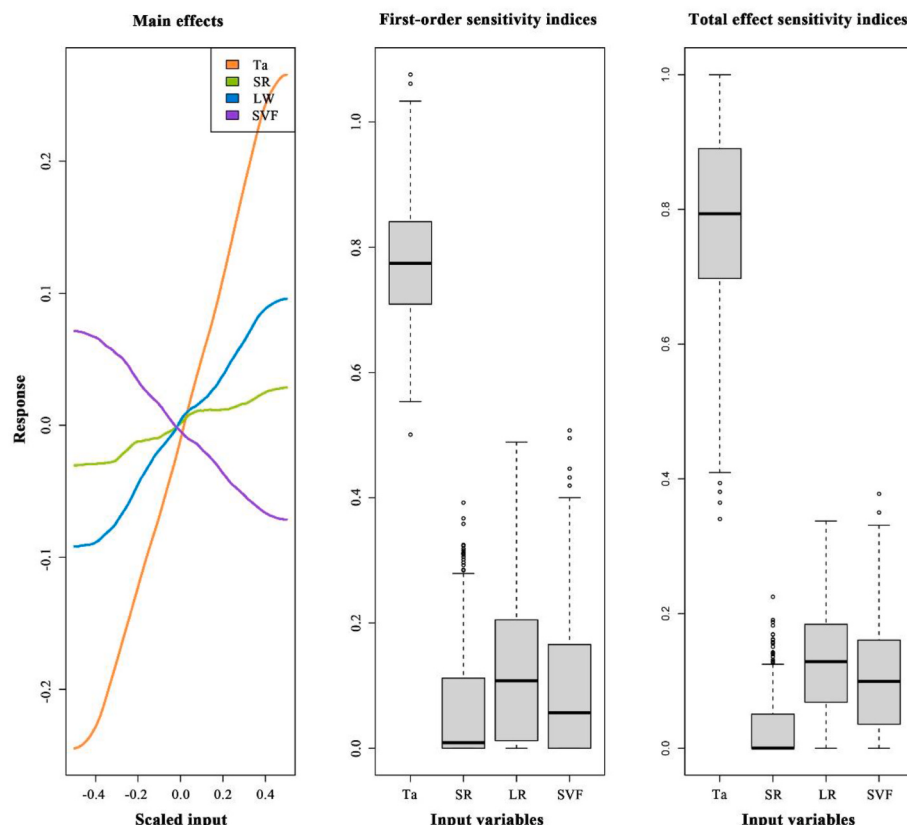
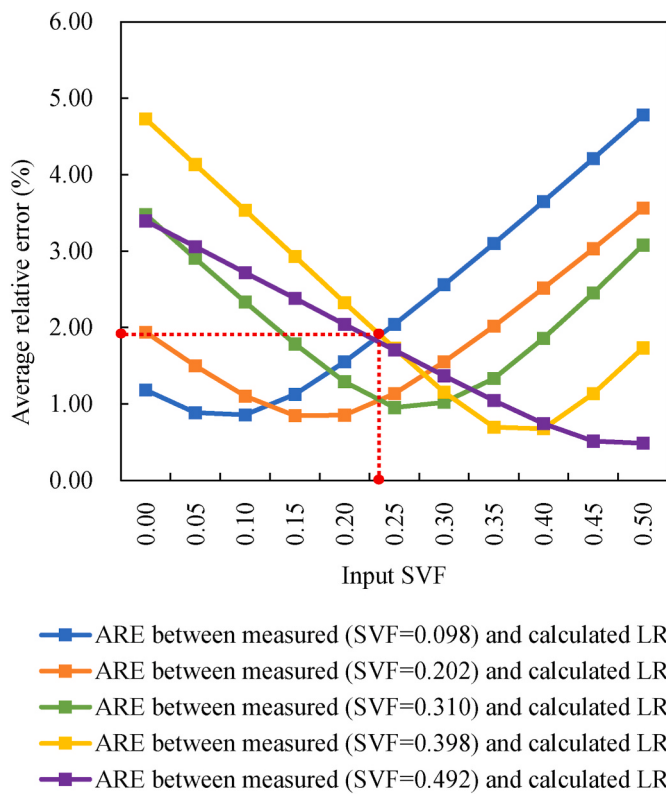


Fig. 6. TGP-based sensitivity analysis of the longwave radiation model.



**Fig. 7.** Quantitative analysis of the influence of SVF parameters on the model output (evaluated with the metric of the average relative error).

#### 3.4. Model accuracy validation

The accuracy of the longwave radiation model was verified. The original model is the algorithm built into the building simulation software EnergyPlus [22]; the simplified model is the one obtained by using the model fitted in this research and setting the SVF input value to 0.236, and the actual SVF model uses the measured SVF values for different scenarios as input values. A comparison between the three models and differences between the calculated and measured values are shown in Fig. 8.

The calculated values of the original model significantly underestimate the measured values, especially in the case of large longwave radiation (Fig. 8(a)). As a result, errors in the calculation of longwave radiation by the original model are large (RMSE of  $18.50 \text{ W m}^{-2}$  and MAPE of 3.10%). In contrast, Fig. 8(b) shows that the accuracy of the calculation in the actual SVF model is significantly improved (RMSE and MAPE of  $4.80 \text{ W m}^{-2}$  and 0.73% for the calculation of longwave

radiation, respectively).

The accuracy of longwave radiation calculations is also higher in the simplified model than in the original model. However, compared with the actual SVF model, the RMSE and MAPE of the simplified model are higher ( $5.29 \text{ W m}^{-2}$  and 0.83%, respectively). This indicates that while the process of simplifying the SVF leads to a decrease in the accuracy of model calculations, the decrease is not significant, and the resulting error is still within acceptable levels. Consequently, this simplified model can be used to address the problem of variation in the availability of the input SVF parameter.

The calculated results for the different model evaluation metrics are summarized in Table 6. In terms of RMSE metrics, the new simplified model is 71.4% more accurate compared with the original model. As a result, the use of the model allows for more accurate calculations of longwave radiation.

In addition, the applicability of the longwave radiation model was verified. The results of the sensitivity analysis showed that temperature is the most influential parameter. As the data used for the fit were obtained through field measurements during the summer when temperatures were higher, data collected in the autumn and spring, when the temperatures were lower, were used to validate the model. Both the autumn and spring longwave radiation and air temperature data used for model validation significantly differed from data collected in the summer, and the results of the model validation are shown in Fig. 9.

Fig. 9 shows that the values calculated by the longwave radiation model are in good agreement with the measured values. Although all the data points do not fit exactly on the diagonal of the XY-axis, the error between the calculated and measured values does not vary substantially depending on the amount of longwave radiation. This indicates that the model has good accuracy for assessing longwave radiation.

The MBE, RMSE, and MAPE for longwave radiation calculated by the validation data were  $-1.99 \text{ W m}^{-2}$ ,  $6.75 \text{ W m}^{-2}$ , and 1.26%, respectively (Table 6). According to the results of the model validation, our longwave radiation model has less computational error than that of the all-sky longwave radiation model proposed by Li et al. [51].

#### 4. Discussion

The field measurements were carried out in Guangzhou, a region

**Table 6**  
Calculation results of evaluation metrics for model validation.

Methods	Evaluation metrics		
	MBE ( $\text{W}\cdot\text{m}^{-2}$ )	RMSE ( $\text{W}\cdot\text{m}^{-2}$ )	MAPE (%)
Original model	15.07	18.50	3.10
Actual SVF model	1.64	4.80	0.73
Simplified model	0.39	5.29	0.83
Validation	-1.99	6.75	1.26

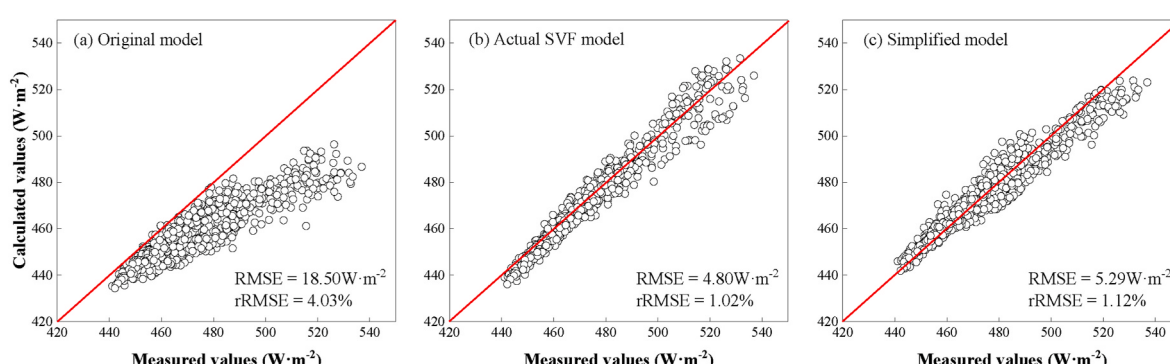


**Fig. 8.** Comparison of measured values and calculated values using different models: (a) original model; (b) modified model with actual SVF; (c) modified model with universal SVF.

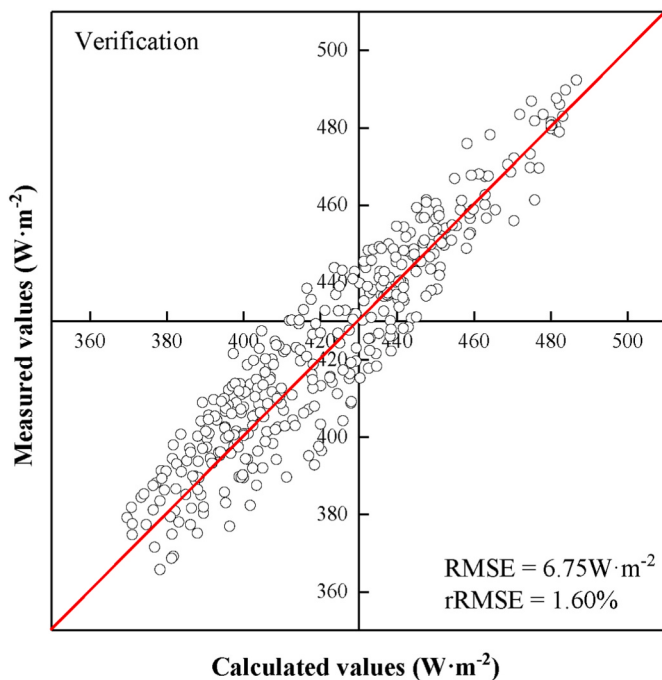


**Fig. 9.** Comparison of the values calculated by the simplified model and measured values obtained in the autumn and spring.

with a typical subtropical climate. The maximum value of the air temperature during the field measurements reached 35.93 °C. However, Colston et al. [58] obtained maximum air temperatures of 29.9 and 29 °C from weather stations in two subtropical regions, South Africa and Nepal, respectively. This indicates that the maximum air temperature in summer is higher in Guangzhou than in other subtropical regions. As longwave radiation is very sensitive to temperature, the results of this study have implications for studies of the properties of longwave radiation.

Based on the concept of equivalent temperature, the parameter of ambient equivalent temperature has been developed for the rapid assessment of longwave radiation emitted by different objects in complex environments. Another similar specific application is the use of the sky effective temperature to quantify the ability of sky domes to emit longwave radiation, as in the case of the clear sky radiation models proposed by Swinbank [59] and Garg [60], which are both based on this concept. In previous studies, this parameter of ambient equivalent temperature is usually directly replaced by the air temperature from meteorological parameters [61]. However, during the daytime, the surface temperature of objects in the surrounding environment is higher than the air temperature due to the heat effect of solar radiation. Therefore, the ambient equivalent temperature in this study was fitted using the data of air temperature and solar radiation to determine an empirical formula applicable to subtropical regions. Compared with the equation obtained by Cheng et al. [51] for a fixed SVF scene, this empirical formula can be more widely applied to different SVF scenes.

Although the energy balance of the building façade has been modelled accordingly, a plausible interpretation of the model output is lacking. Therefore, a sensitivity analysis was performed to determine the uncertainty of different input parameters when calculating longwave radiation of building façades, and a universal SVF value was proposed to simplify the inputs of the model. The model proposed in this study can accurately calculate the longwave radiation emitted by the environment without SVF input, compared with a model that directly divides the sky and ground into 0.5 [15]. This method solves the problem of the difficulty of obtaining SVF parameters in existing building simulation software when calculating longwave radiation exchanges. The simplified

model improves the accuracy of the longwave radiation calculation by 71.4% compared with the original model built into Energyplus software. Similarly, the results of Luo et al. [24] and Xie et al. [25] demonstrate that optimized calculations of longwave radiation can more accurately predict building cooling and heating energy demand.

## 5. Conclusions

In the present study, the concept of ambient equivalent temperature was proposed for evaluating the longwave radiation exchange of building façades in a complex environment (i.e., an environment containing other buildings and trees). This parameter allows the longwave radiation emitted by the urban environment with a high density of buildings to be quantified more efficiently. Furthermore, the analysis of meteorological parameters revealed that air temperature and solar radiation are important parameters that determine the ability of the environment to emit longwave radiation. Thus, the relationships between the ambient equivalent temperature and meteorological parameters were established through multiple linear regression to simplify the input parameters of the model.

The longwave radiation transfer model of building façades was developed by considering the exchange of longwave radiation between buildings and the environment, and its applicability was improved by simplifying the input parameters. Although the SVF parameter has a significant influence on the solar heat gain of a building façade, its influence on the energy balance of longwave radiation remains unclear. Therefore, an important contribution of this work was characterizing the influence of the SVF parameter on calculations of longwave radiation of the building façade. A sensitivity analysis was conducted to evaluate all input parameters of the longwave radiation model, and a quantitative analysis was performed to clarify the influence of SVF on the accuracy of calculations. Temperature was the most important parameter affecting the longwave radiation exchange of the building façade, and the influence of SVF was smaller by comparison. As a result, a universal value for SVF was determined to minimize the calculation error of the longwave radiation transfer model.

The accuracy of the model was verified using various evaluation metrics. Compared with the original model, the accuracy of the longwave radiation calculation of the simplified model proposed in this paper was improved by 71.4%; our model thus permits more accurate calculations of the longwave radiation exchange of building façades. This facilitates a more detailed analysis of the longwave heat exchange between buildings and the environment in studies of urban modelling. Such analyses are also important for effectively assessing the adverse effects of excessive heat radiation in the built environment due to increased temperatures on the environment and human comfort.

As the longwave radiation model proposed in this study was developed in a hot and humid climate, the applicability of this model to other regions with sub-zero temperatures and dry climates requires evaluation. Furthermore, although field measurements were carried out in six different SVF scenes, only two of the measurement locations were on actual building façades. Therefore, additional experiments on actual building façades are required to validate the calculation method for incident longwave radiation. The potential limitations mentioned above will be further refined in future studies to improve the applicability of the longwave radiation model.

## CRediT authorship contribution statement

**Cheng Zhao:** Writing – review & editing, Writing – original draft, Validation, Methodology, Investigation, Formal analysis, Data curation, Conceptualization. **Lei Zhang:** Supervision, Resources, Project administration, Funding acquisition, Conceptualization. **Yu Zhang:** Resources, Funding acquisition.

## Declaration of competing interest

The authors declare that they have no known competing financial interests or personal relationships that could have appeared to influence the work reported in this paper.

## Data availability

Data will be made available on request.

## Acknowledgments

This project was supported by the National Natural Science Foundation of China (No. 52178075).

## References

- [1] International Energy Agency, WEO-2015 Special Report: Energy and Climate Change, IEA, Paris, France, 2015.
- [2] C.O. Pedersen, D.E. Fisher, R.J. Liesen, Development of a Heat Balance Procedure for Calculating Cooling Loads (No. CONF-970668-), American Society of Heating, Refrigerating and Air-Conditioning Engineers, Inc., Atlanta, GA (United States), 1997.
- [3] M. Dave, B. Watson, D. Prasad, Performance and perception in prefab housing: an exploratory industry survey on sustainability and affordability, *Procedia Eng.* 180 (2017) 676–686.
- [4] M.S. Tokarik, A Multi-Objective Optimization Analysis of Passive Energy Conservation Measures in A Toronto House, Ryerson University, MASc. Thesis, 2011.
- [5] S. Naji, L. Aye, M. Noguchi, Sensitivity analysis on energy performance, thermal and visual discomfort of a prefabricated house in six climate zones in Australia, *Appl. Energy* 298 (2021), 117200.
- [6] H.S. Hens, Building Physics-Heat, Air and Moisture: Fundamentals and Engineering Methods with Examples and Exercises, John Wiley & Sons, 2017.
- [7] Y.C. Chen, H.W. Chiu, Y.F. Su, Y.C. Wu, K.S. Cheng, Does urbanization increase diurnal land surface temperature variation? Evidence and implications, *Landscape Urban Plann.* 157 (2017) 247–258.
- [8] M. Santamouris, N. Papanikolaou, I. Livada, I. Koronakis, C. Georgakis, A. Argiriou, D.N. Assimakopoulos, On the impact of urban climate on the energy consumption of buildings, *Sol. Energy* 70 (3) (2001) 201–216.
- [9] A. Gros, E. Bozonnet, C. Inard, Modelling the radiative exchanges in urban areas: a review, *Adv. Build. Energy Res.* 5 (1) (2011) 163–206.
- [10] T. Hong, Y. Chen, X. Luo, N. Luo, S.H. Lee, Ten questions on urban building energy modeling, *Build. Environ.* 168 (2020), 106508.
- [11] R.J. Cole, The longwave radiative environment around buildings, *Build. Environ.* 11 (1) (1976) 3–13.
- [12] J. Allegrini, V. Dorer, J. Carmeliet, Influence of the urban microclimate in street canyons on the energy demand for space cooling and heating of buildings, *Energy Build.* 55 (2012) 823–832.
- [13] J. Allegrini, V. Dorer, J. Carmeliet, Impact of radiation exchange between buildings in urban street canyons on space cooling demands of buildings, *Energy Build.* 127 (2016) 1074–1084.
- [14] L. Da-long, Z. Hui-hui, L. Jia-ping, Rule of long-wave radiation in enclosed building space, *Energy Build.* 182 (2019) 311–321.
- [15] D. Mazzeo, N. Matera, C. Cornaro, G. Oliveti, P. Romagnoni, L. De Santoli, EnergyPlus, IDA ICE and TRNSYS predictive simulation accuracy for building thermal behaviour evaluation by using an experimental campaign in solar test boxes with and without a PCM module, *Energy Build.* 212 (2020), 109812.
- [16] L. Evangelisti, C. Guattari, F. Asdrubali, On the sky temperature models and their influence on buildings energy performance: a critical review, *Energy Build.* 183 (2019) 607–625.
- [17] M. Yadav, A.K. Berwal, Predicting building wall temperature in composite climate using regression models: a comparative study, *Mater. Today Proc.* 45 (2021) 5052–5058.
- [18] K. Zhang, A. Garg, G. Mei, M. Jiang, H. Wang, S. Huang, L. Gan, Thermal performance and energy consumption analysis of eight types of extensive green roofs in subtropical monsoon climate, *Build. Environ.* 216 (2022), 108982.
- [19] G. Tsilingiridis, K. Papakostas, Investigating the relationship between air and ground temperature variations in shallow depths in northern Greece, *Energy* 73 (2014) 1007–1016.
- [20] B.D. Miller, K.R. Carter, S.C. Reed, T.E. Wood, M.A. Cavalieri, Only sun-lit leaves of the uppermost canopy exceed both air temperature and photosynthetic thermal optima in a wet tropical forest, *Agric. For. Meteorol.* 301 (2021), 108347.
- [21] P.K. Cheung, C.Y. Jim, P.L. Hung, Preliminary study on the temperature relationship at remotely-sensed tree canopy and below-canopy air and ground surface, *Build. Environ.* 204 (2021), 108169.
- [22] DoE, U. S., EnergyPlus Engineering Reference: the Reference to EnergyPlus Calculations, Lawrence Berkeley National Laboratory, 2009.
- [23] N.L. Jones, D.P. Greenberg, Fast computation of incident solar radiation from preliminary to final building design, in: Proceedings of the 12th Conference of International Building Performance Simulation Association, 2011, November, pp. 14–16. Sydney, Australia.
- [24] X. Luo, T. Hong, Y.H. Tang, Modeling thermal interactions between buildings in an urban context, *Energies* 13 (9) (2020) 2382.
- [25] X. Xie, Z. Luo, S. Grimmond, T. Sun, W. Morrison, Impact of inter-building longwave radiative exchanges on building energy performance and indoor overheating, *Build. Environ.* 209 (2022), 108628.
- [26] X. Yang, L. Zhao, M. Bruse, Q. Meng, An integrated simulation method for building energy performance assessment in urban environments, *Energy Build.* 54 (2012) 243–251.
- [27] C. Miller, D. Thomas, J. Kämpf, A. Schlueter, Long wave radiation exchange for urban scale modelling within a co-simulation environment, in: Proceedings of International Conference CISBAT 2015 Future Buildings and Districts Sustainability from Nano to Urban Scale (No. CONF, LESO-PB, EPFL, 2015, pp. 871–876.
- [28] R. Evans, V. Dorer, J. Carmeliet, Simulating external longwave radiation exchange for buildings, *Energy Build.* 75 (2014) 472–482.
- [29] C. Feng, Y. Lei, X. Huang, W. Zhang, Y. Feng, X. Zheng, Experimental and theoretical analysis of sub-ambient cooling with longwave radiative coating, *Renew. Energy* 193 (2022) 634–644.
- [30] T.L. Bergman, T.L. Bergman, F.P. Incropera, D.P. Dewitt, A.S. Lavine, Fundamentals of Heat and Mass Transfer, John Wiley & Sons, 2011.
- [31] I. Sosorova, M. Angulo, P. Bahrami, B. Stephens, A model of vegetated exterior facades for evaluation of wall thermal performance, *Build. Environ.* 67 (2013) 1–13.
- [32] F. Convertino, G. Vox, E. Schettini, Thermal barrier effect of green façades: long-wave infrared radiative energy transfer modelling, *Build. Environ.* 177 (2020), 106875.
- [33] G.N. Walton, Thermal Analysis Research Program Reference Manual, National Bureau of Standards, March, 1983.
- [34] G. Clark, C. Allen, The estimation of atmospheric radiation for clear and cloudy skies, in: Proc. 2nd National Passive Solar Conference, 1978, March, pp. 675–678 (AS/ISES).
- [35] S.A. Klein, TRNSYS-A Transient System Simulation Program, University of Wisconsin-Madison, Engineering Experiment Station Report, 1988, 38-12.
- [36] Y. Han, J.E. Taylor, Disaggregate analysis of the inter-building effect in a dense urban environment, *Energy Proc.* 75 (2015) 1348–1353.
- [37] M. Dirksen, R.J. Ronda, N.E. Theeuwes, G.A. Pagani, Sky view factor calculations and its application in urban heat island studies, *Urban Clim.* 30 (2019), 100498.
- [38] L. Zeng, J. Lu, W. Li, Y. Li, A fast approach for large-scale Sky View Factor estimation using street view images, *Build. Environ.* 135 (2018) 74–84.
- [39] C. Miao, S. Yu, Y. Hu, H. Zhang, X. He, W. Chen, Review of methods used to estimate the sky view factor in urban street canyons, *Build. Environ.* 168 (2020), 106497.
- [40] L. Chen, E. Ng, X. An, C. Ren, M. Lee, U. Wang, Z. He, Sky view factor analysis of street canyons and its implications for daytime intra-urban air temperature differentials in high-rise, high-density urban areas of Hong Kong: a GIS-based simulation approach, *Int. J. Climatol.* 32 (1) (2012) 121–136.
- [41] X. Li, C. Ratti, I. Seiferling, Quantifying the shade provision of street trees in urban landscape: a case study in Boston, USA, using Google Street View, *Landscape Urban Plann.* 169 (2018) 81–91.
- [42] W.S. Rasband, ImageJ, U. S., & National Institutes of Health, 2015, pp. 1997–2018. Bethesda, Maryland, USA, <https://imagej.nih.gov/ij/>. URL.
- [43] A. Saltelli, M. Ratto, T. Andres, F. Campolongo, J. Cariboni, D. Gatelli, S. Tarantola, Global Sensitivity Analysis: the Primer, John Wiley & Sons, 2008.
- [44] A. Saltelli, Sensitivity analysis: could better methods be used? *J. Geophys. Res. Atmos.* 104 (D3) (1999) 3789–3793.
- [45] W. Tian, A review of sensitivity analysis methods in building energy analysis, *Renew. Sustain. Energy Rev.* 20 (2013) 411–419.
- [46] W. Tian, P. De Wilde, Uncertainty and sensitivity analysis of building performance using probabilistic climate projections: a UK case study, *Autom. ConStruct.* 20 (8) (2011) 1096–1109.
- [47] W. Tian, R. Choudhary, A probabilistic energy model for non-domestic building sectors applied to analysis of school buildings in greater London, *Energy Build.* 54 (2012) 1–11.
- [48] R.B. Gramacy, M. Taddy, Categorical Inputs, Sensitivity Analysis, Optimization and Importance Tempering with Tgp Version 2, an R Package for Treed Gaussian Process Models, University of Cambridge Statistical Laboratory Tech. Rep., 2009.
- [49] L. Zhu, J. Zhang, Y. Gao, W. Tian, Z. Yan, X. Ye, C. Wu, Uncertainty and sensitivity analysis of cooling and heating loads for building energy planning, *J. Build. Eng.* 45 (2022), 103440.
- [50] W. Tian, Y. Heo, P. De Wilde, Z. Li, D. Yan, C.S. Park, G. Augenbroe, A review of uncertainty analysis in building energy assessment, *Renew. Sustain. Energy Rev.* 93 (2018) 285–301.
- [51] M. Li, Y. Jiang, C.F. Coimbra, On the determination of atmospheric longwave irradiance under all-sky conditions, *Sol. Energy* 144 (2017) 40–48.
- [52] C. Zhao, L. Zhang, Y. Yang, Y. Zhang, M. Liu, J. Yan, L. Zhao, Long-wave infrared radiation properties of vertical green façades in subtropical regions, *Build. Environ.* 223 (2022), 109518.
- [53] J. Ge, Y. Wang, H. Akbari, D. Zhou, The effects of sky view factor on ground surface temperature in cold regions—A case from Xi'an, China, *Build. Environ.* 210 (2022), 108707.
- [54] M. Ouzzane, P. Eslami-Nejad, M. Badache, Z. Aidoun, New correlations for the prediction of the undisturbed ground temperature, *Geothermics* 53 (2015) 379–384.

- [55] W. Pereira, A. Bögl, T. Natschläger, Sensitivity analysis and validation of an EnergyPlus model of a house in Upper Austria, *Energy Proc.* 62 (2014) 472–481.
- [56] J.L. Loepky, J. Sacks, W.J. Welch, Choosing the sample size of a computer experiment: a practical guide, *Technometrics* 51 (4) (2009) 366–376.
- [57] J. Cariboni, D. Gatelli, R. Liska, A. Saltelli, The role of sensitivity analysis in ecological modelling, *Ecol. Model.* 203 (1–2) (2007) 167–182.
- [58] J.M. Colston, T. Ahmed, C. Mahopo, G. Kang, M. Kosek, F. de Sousa Junior, M. E. The, Evaluating meteorological data from weather stations, and from satellites and global models for a multi-site epidemiological study, *Environ. Res.* 165 (2018) 91–109.
- [59] W.C. Swinbank, Long-wave radiation from clear skies, *Q. J. R. Meteorol. Soc.* 89 (381) (1963) 339–348.
- [60] H.P. Garg, Treatise on Solar Energy, John Wiley & Sons, 1982.
- [61] T. Šuklje, S. Medved, C. Arkar, On detailed thermal response modeling of vertical greenery systems as cooling measure for buildings and cities in summer conditions, *Energy* 115 (2016) 1055–1068.